Egypt. J. Chem. **Vol. 67**, No. 9 pp. 381 - 392 (2024)

Egyptian Journal of Chemistry

http://ejchem.journals.ekb.eg/

Influence of Different Processes on Corrosion Performance of Al 1070 Alloy in Chloride Media

Ghalia A. Gaber[1], Lamiaa Z. Mohamed[2,*], Walaa Abd-ElaAziem[3]

[1]*Department of Chemistry, Faculty of Science (Girls), Al-Azhar University, P.O. Box: 11754, Yousef Abbas Str., Nasr City, Cairo, Egypt*

[2]*Mining, Petroleum, and Metallurgical Engineering Department, Faculty of Engineering, Cairo University, Giza, 12613, Egypt.*

[3]*Department of Mechanical Design and Production Engineering, Faculty of Engineering, Zagazig University, P.O. Box 44519, Egypt*

Abstract

Al 1070 alloy pins were subjected to four passes of micro/meso-scale equal channel angular pressing at room temperature in the current work. The channel diameter of 1.5 mm is the smallest channel diameter ever obtained in meso-scale processing. The effect of Al 1070 alloy processes on corrosion behavior in 3.5%NaCl and different concentrations of HCl solutions was investigated. The investigated alloy was processed by ECAP by four passes and different speeds of extrusion. Corrosion assessments were carried out by chemical technique (weight-loss method) in 3.5%NaCl, 0.2M HCl, and 1M HCl for two different times of 1h and 4h. The highest corrosion resistance is for one pass ECAP in HCl solutions. Among the different extrusion speeds, the samples with an extrusion speed of 1 mm/min demonstrated the lowest corrosion rate across all tested environments. The average grain sizes of 28.77 and 22.67 μm correspond to the extrusion speeds of 1 and 15 mm/min, respectively. As the extrusion speed increases, the grain size decreases. The surface morphology of the corroded Al 1070 alloy was further examined using scanning electron microscopy (SEM). Pitting corrosion was observed in all surface morphologies, highlighting the susceptibility of the alloy to this form of corrosion under the investigated conditions.

Keywords: Extrusion speed, Al 1070 Alloy; Corrosion behavior; Chloride media; Microstructure.

1. Introduction

Researchers and engineers have recently focused their attention on the possibility of products in several contemporary industrial domains, including communications, electronics, biomedical, optics, and more, to achieve high functionality, high reliability, and the production of micro-parts. The micro/meso-scale forming method is one of the most attractive micro-manufacturing techniques due to its rapid production rate, low cost, superior mechanical properties, and ability to produce small, complex metallic components with near-net forms, among other benefits [1-3]. However, since the theory of micro/meso-forming processes differs from those in the macro-scale, the primary obstacle in the micro-forming of metallic parts is the occurrence of diverse mechanical size effects. Stated differently, certain intrinsic characteristics of the micro-component, such as the surface roughness and grain size, cannot be reduced in conjunction with the geometric ones when the part is miniaturized in terms of its geometric dimensions [3, 4]. A unique material response and a higher likelihood of failure during fabrication, for example, can arise from the micro/meso-forming of metal parts made of a few grains as opposed to a

*Corresponding author e-mail: lamiaa.zaky@cu.edu.eg ; (Lamiaa Z. Mohamed).
Received date 03 January 2024; revised date 20 February 2024; accepted date 03 March 2024
DOI: 10.21608/EJCHEM.2024.260371.9138

polycrystalline material. Vollertsen et al. [5, 6] and Geiger et al. [4] provided a thorough analysis of the metal micro-forming methods, their uses, and their drawbacks.

Materials with ultrafine grains (UFGs) show excellent formability and distinctive mechanical qualities [7]. Additionally, it has an impact on the processed micro-components surface quality [8, 9]. The severe plastic deformation (SPD) method that is thought to be most suitable for creating ultra-fine-grained (UFG) materials is equal channel angular pressing (ECAP). As a result, in this work, fine-grained material of microscopic pins was produced using micro/meso-scale ECAP (MMS-ECAP) with a die channel diameter of 1.5 mm which is the smallest diameter ever achieved. Previous papers [10–13] covered the MMSECAP die's design and guiding concepts in detail.

In the automotive sector, new materials and manufacturing techniques are created to address the growing environmental and financial issues associated with lightweight. High mechanical strength, high conductivity, and great corrosion resistance are all necessary for automobile wires [14]. Al and its alloys are widely used in a variety of rail, automotive, aerospace, and marine applications owing to their lightweight nature. For the last twenty years, materials scientists have been interested in aluminum and its alloy samples with fine-grain microstructures, which can result in a noticeable improvement in the physical and mechanical characteristics. These specifications are met by Al-Mg-Si alloys, which are already in use for automotive wire applications [14]. The traditional method of producing aluminum wires involves alternating stages of heat treatments and deformation (drawing). Unfortunately, Al wires need larger sections to carry the same amperage as copper wires because Al alloys are less conductive than copper. ECAP is currently a widely used method among them to produce UFG microstructures with significantly improved mechanical characteristics [15–20]. In ECAP, a bar is pressed through a die at a specific angle. Without altering the material's cross-section, it imparts significant strain by shear deformation [21]. In AA 6060 T6, Khelfa et al. found that a single ECAP pass resulted in a 97% reduction in grain size [22]. Tissue changes during ECAP processing in Al-Mg-Si alloy were demonstrated by Sitdikov et al. [23]. It is now evident that SPD significantly alters fundamental microstructural characteristics such as texture, boundary nature, and grain size and shape. Moreover, SPD methods that have been demonstrated to be successful in fragmenting intermetallic coarse particles (IMCs) can also have an impact on IMCs [24]. The ability to combine heat treatments and high strain to improve precipitation kinetics and optimize the mechanical and electrical characteristics of Al-Mg-Si alloys is yet another intriguing aspect of ECAP. For instance, Murashkin et al. succeeded in obtaining ß' hardening precipitates in AA 6101 during ECAP at 130 °C [16]. In comparison to standard thermo-mechanical treatments of Al-Mg-Si alloys, they observed an increase in the samples' mechanical strength and electrical conductivity. These microstructural alterations may significantly impact how Al alloys treated by ECAP behave in terms of corrosion. It is a well-known fact that the precipitates included in aluminum alloys have a significant influence on their corrosion behavior. The literature [25–27] has examined the function of intergranular ß-Mg_2Si precipitates that may have evolved during the aging of Al–Mg–Si alloys. The exploration of corrosion characteristics at the meso-scale has received limited attention in the existing literature. In this current study, our primary emphasis is placed on a comprehensive examination of the influence of various processing techniques on the corrosion characteristics of Al 1070 alloy in 3.5% NaCl, 0.2M HCl, and 1.0M HCl solutions, with a particular focus on different immersion periods, 1 h and 4 h. Our investigation extends beyond the mere quantification of corrosion rates, delving into a nuanced understanding of the intricate relationship between processing methods and the resulting corrosion behavior. Additionally, a thorough analysis of surface morphologies post-corrosion has been undertaken, aiming to elucidate any distinctive features or patterns that may offer insights into the underlying mechanisms of corrosion in meso-scale conditions. This comprehensive approach seeks to contribute valuable insights to the existing body of knowledge on meso-scale corrosion characteristics, filling a crucial gap in the current literature.

2. Experimental work

In the current work, ambient temperature micro/meso-scale ECAP was used to process Al 1070 alloy specimens measuring 1.5 mm in diameter. Because the Al 1070 alloy is widely used in electrical and electronic applications, it was chosen for this

study. The Al 1070 alloy, as received, was a 1.5 mm x 300 mm wrought rod with a weight percentage of 0.25 Fe, 0.2 Si, 0.04 Zn, 0.04 Cu, and Al. The specimens were heat-treated at 350 °C at a heating rate of 1.5 °C/s to remove any prior work-hardening effects of the as-received Al rods. They were then cooled at 0.3 °C/s to room temperature (RT). ECAP procedures were carried out using route B_C for up to four ECAP passes at RT and a displacement rate of 1 mm/min.

The weight-loss (WL) method was used to examine the corrosion behavior of the Al 1070 alloy. Industrial tests are conducted using chloride-containing solutions, such as de-icing salts, which are the most realistic of the automobile environment [14]. Although there are other contaminants, the purpose of this paper was not to examine their effects. To compare the results with immersion in 3.5% NaCl (pH=6.8), the corrosion experiments were conducted in an extremely aggressive electrolyte, namely 0.2 M HCl (pH=1.7) and 1.0 M HCl (pH=0.8) solutions.

After being ground using emery paper grades up to 2000, the various samples under various conditions were polished using alumina paste. After being cleaned with tap water and then twice-distilled water, they were air-dried and further cleaned with acetone. To ensure accuracy, each specimen was dried using hot air and weighed using an analytical balance. After the specimen weights were measured, they were placed at RT into solutions containing 3.5% NaCl, 0.2 M HCl, and 1.0 M HCl. The weights were noted at one and 4 h. The corrosion rate (CR) values were computed by measuring the variations in weights at each interval. Eqs. 1 and 2 were used to compute the CR of Al 1070 alloys under various circumstances in $cm^{-2}.hr^{-1}$ based on the WL data [28, 29].

$$\Delta W = W_1 - W_2 \quad (1)$$

$$CR\ (mm/y) = \frac{\Delta W * K}{A * T * D} \quad (2)$$

Where W_1 and W_2 are the coupon's weight before/after immersion in the corroding medium respectively. K denotes constant, A is the submerged area, T is the immersed time, and D is the density of Al 1070 alloy.

The morphology after corrosion of the Al 1070 alloy was analyzed using a scanning electron microscope (SEM) to evaluate its corrosion performance.

3. Results and Discussion

3.1. Al 1070 Alloy Microstructure

The Al 1070 alloy microstructure maps of both before/after MMS-ECAP passes are displayed in Fig. 1. The undeformed material microstructure exhibits equiaxed grain morphology, with an average grain size of around 20.4 μm and a very uniform distribution, as seen in Fig. 1(a). Following the first ECAP pass, grain refining begins, and the microstructure shows a heterogeneous structure made up of a mixture of fine and coarse grains. The microstructure was found to have significantly improved after the fourth ECAP run, going from roughly 20 μm (the original undisturbed sample) to almost 2 μm. This is explained by the progressive process of grain subdivision, which turns low-angle grain borders into high-angle grain boundaries. Therefore, the grain subdivision mechanism is responsible for the higher degree of grain refinement of the treated Al 1070 alloy as determined by the MMS-ECAP. Our earlier works provide additional details regarding the mechanism of aluminum grain subdivision

.

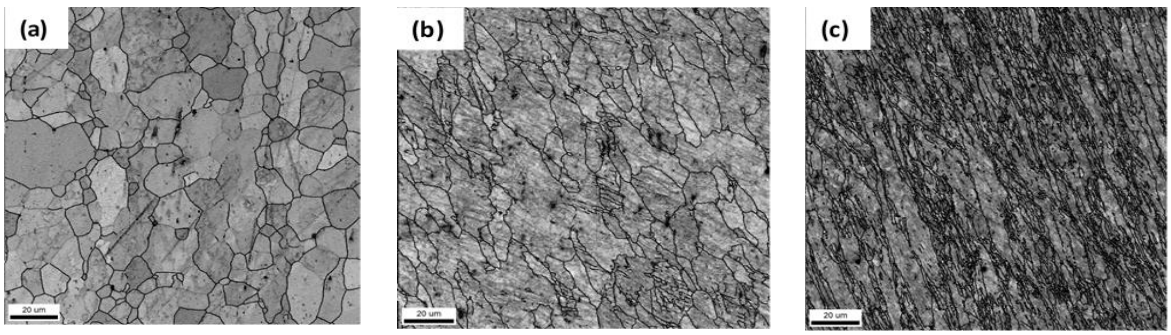

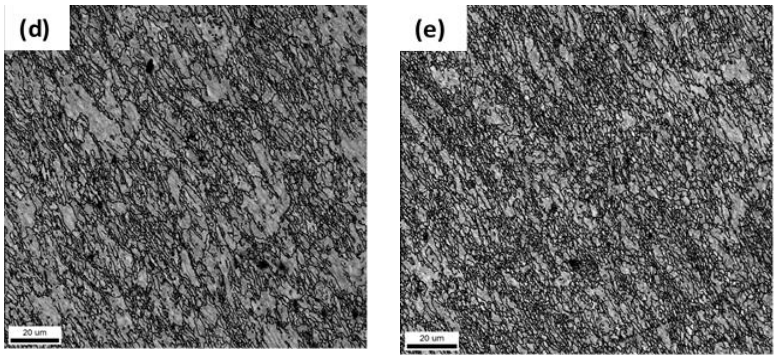

Fig. 1. Microstructure of Al 1070 alloy in the longitudinal direction: (a) annealed; (b) 1 ECAP pass; (c) 2 ECAP passes (d) 3 ECAP passes and (e) 4 ECAP passes.

The grain boundary maps of samples extruded at two different rates, 15 mm/min and 1 mm/min, are displayed in Fig. 2 (a). It is discovered that the extrusion speed has an impact on the grain size of Al 1070 alloy. The extrusion speeds of 1 and 15 mm/min, respectively, correspond to the average grain sizes of 28.77 and 22.67 μm. Consequently, the grain size reduces as the extrusion speed rises. Our prior work [30] provides data on the mechanisms of grain refinement at various RAM speeds.

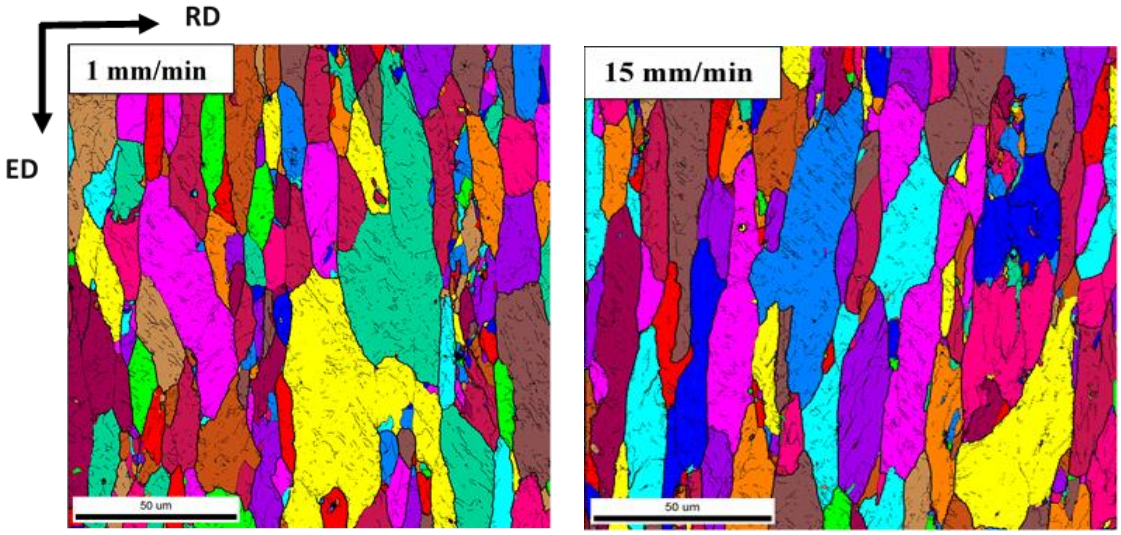

Fig. 2. (a) Grain boundary of Al 1070 alloy extruded at two different speeds, 1mm/min, and 15 mm/min. ED is the extrusion direction and RD radial direction.

3.2. Corrosion Behavior

3.2.1. Influence of ECAP on the corrosion behavior of Al 1070 alloy

Fig. 3 illustrates the CR values obtained through the WL technique for Al 1070 alloy in the transverse direction under various conditions, including annealed, 1 pass, 2 passes, 3 passes, and 4 passes of ECAP, tested in 0.2M HCl and 1.0M HCl at RT. The findings highlight the importance of considering two scenarios to comprehend the influence of grain size on corrosion resistance. The first scenario pertains to materials exhibiting active corrosion, while the second pertains to materials with low to passive dissolving rates. The observed variations in CR due to ECAP, which can either increase or decrease corrosion rates, contribute to resolving debates surrounding its impact on the corrosion behavior of Al alloys [31-36]. Moreover, the diversity in interfaces, particularly their degree of disorientation, may elucidate the challenge of establishing a direct correlation between corrosion behavior and grain size. For example, studies have

shown a strong correlation between the distribution of grain boundary disorientation and the susceptibility of Al to intergranular corrosion in HCl [37]. It can be inferred that ECAP enhances pit propagation in both forming and in-depth directions by increasing surface area rather than depth. Additionally, considering the simultaneous increase in both pit width and pit density helps elucidate the observed rise in corroded surface area for ECAP-treated samples [16].

The samples subjected to the ECAP process exhibit a higher pit density compared to the initially received sample. The CR values for the annealed condition and 1, 2, 3, and 4 passes of ECAP, following a 1 h immersion time in 0.2 M HCl, are 1239.9, 82.6, 206.6, 413.3, and 496 mm/y, respectively. For a 4 h immersion time in the 0.2 M HCl concentration, the corresponding CR values are 454.6, 41.3, 113.6, 165.3, and 310.0 mm/y, respectively. In a 1.0 M HCl solution, the CR values for the annealed condition and 1, 2, 3, and 4 passes of ECAP after a 1 h immersion time are 6199.6, 1239.9, 4133.1, 8679.4, and 12399.2 mm/y, respectively. For a 4 h immersion time in the 1.0 M concentration, the CR values are 5579.6, 516.6, 1239.9, 2583.2, and 3926.39 mm/y, respectively.

Observations indicate a correlation between the increasing acidity of the HCl solution and rising CR values. Furthermore, the CR values tend to decrease as immersion time extends from 1 h to 4 h in both concentrations of HCl solutions. This trend suggests the potential formation of a protective layer, contributing to a reduction in CR values. It is noted that the sample from the 1-pass ECAP condition performs the best across all tested conditions. The increase in the number of ECAP passes is known to reduce grain size and enhance mechanical properties like tensile stress and hardness [10-13]. However, this also increases grain boundary area, potentially contributing to the observed rise in CR with an increase in the number of ECAP passes [10, 11].

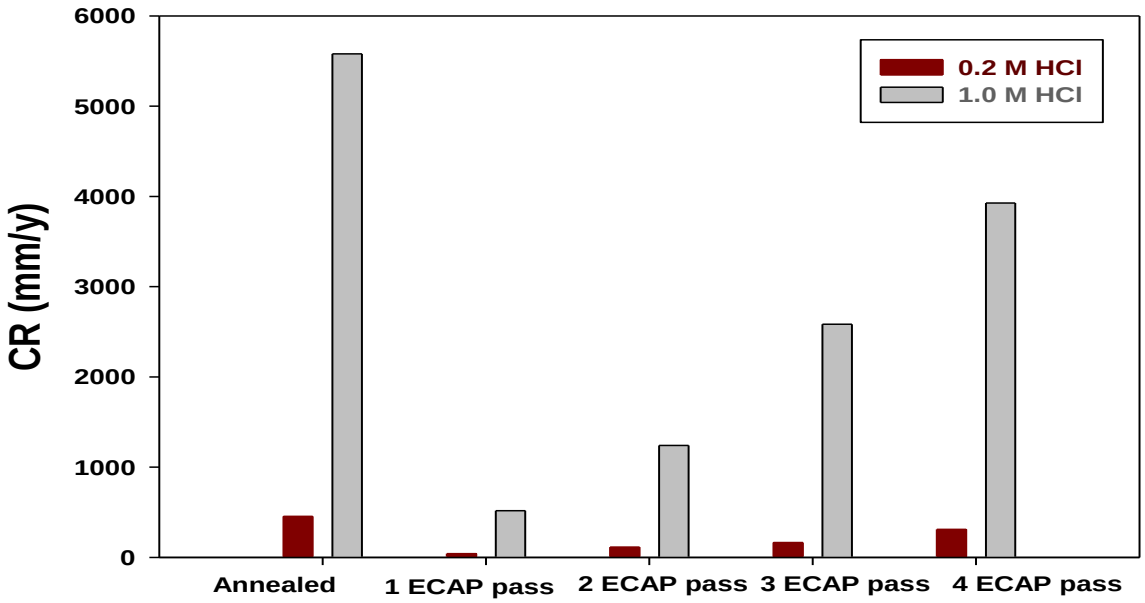

Fig. 3. The CR values for Al 1070 alloy immersed in 0.2M and 1.0M HCl for 4h at RT for annealed condition and different passes of ECAP.

Fig. 4 illustrates the CR values obtained through the WL method for Al 1070 alloy in 3.5% NaCl solution at RT under different processing conditions, including annealed, 1 pass, 2 passes, 3 passes, and 4 passes of ECAP. In the annealed condition in 3.5% NaCl, the CR values are the lowest at both 1 h (454.6 mm/y) and 4 h (206.7 mm/y) immersion times compared to the samples processed using ECAP with different passes. As the number of passes of ECAP increases from one pass to four, the CR values exhibit a rising trend. Specifically, for a 1 h immersion time, the CR values are 909.3, 1033.3, 1239.9, and 1529.2 mm/y for 1 pass, 2 passes, 3 passes, and 4 passes of ECAP, respectively. Extending the immersion time to 4 h results in the formation of an Al_2O_3 protective layer, leading to a decrease in CR values to 299.7, 423.6, 464.9, and 754.3 mm/y for 1 pass, 2 passes, 3 passes, and 4 passes of ECAP, respectively.

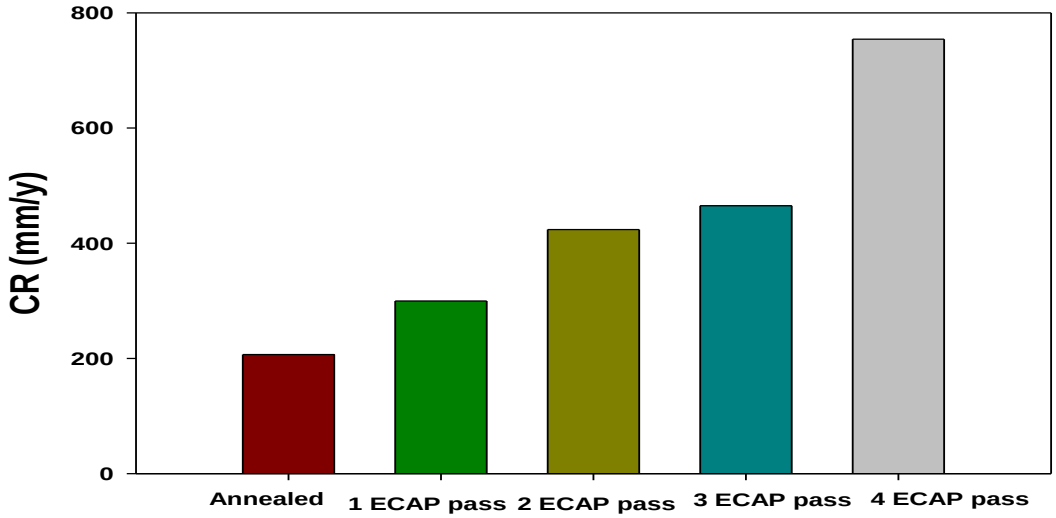

Fig. 4. The CR values for Al 1070 alloy immersed in 3.5%NaCl for 4h at RT for annealed condition and different passes of ECAP.

The surface morphologies of the annealed alloy and the alloy processed with four passes of ECAP, immersed in 1.0M HCl for 4 h at RT, are depicted in Fig. 5. Pitting corrosion is evident in the corroded alloys, with the annealed alloys exhibiting more pronounced pitting compared to the alloy subjected to four passes of ECAP. As shown in Fig. 1, the reduction in Al grain size following ECAP results in more compact crystals within the pitting area. The observed pit morphologies, characterized by a typical faceted-type crystallographic appearance in Fig. 5, seem to intensify with ECAP and are tangentially connected by filaments likely induced by hydrogen development [38–40]. The corrosion resistance is enhanced through ECAP by elevating the oxidation rate of Al to form Al_2O_3 [41, 42]. The rate of Al oxide film formation increases due to the reduction in Al grain size resulting from the ECAP process.[41]

It is observed that one pass of ECAP results in a tenfold reduction in CR compared to annealing in both 0.2M HCl and 1.0M HCl. However, an increase in the number of ECAP passes from one to four leads to a sixfold increase in CR for 0.2M HCl and a sevenfold increase for 1.0M HCl during a 4 h immersion time, as indicated by the WL method. The severe plastic deformation involved in ECAP can induce residual stresses within the material. Residual stresses can affect the initiation and propagation of corrosion cracks. These stresses may lead to localized corrosion and contribute to stress corrosion cracking under certain conditions. The increasing number of ECAP passes may induce internal stresses inside the alloy that are responsible for increasing the corrosion rate [43].

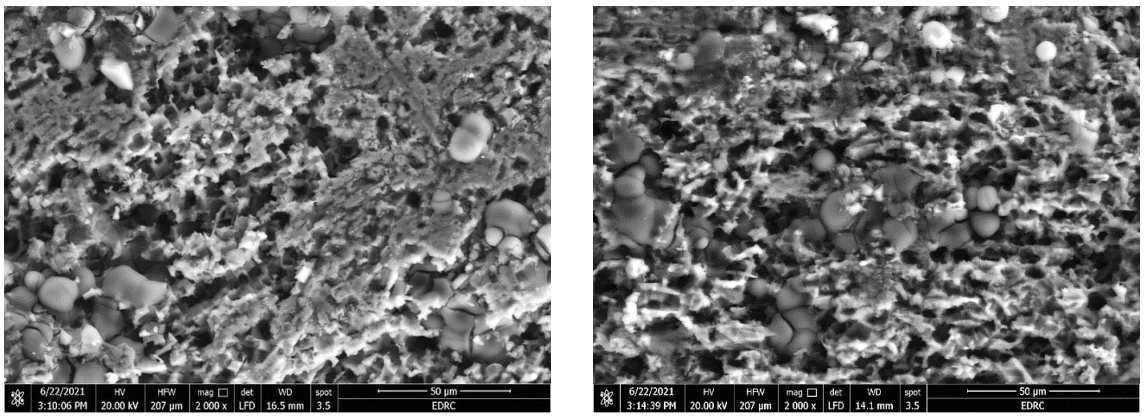

(a) (b)

Fig. 5. Surface morphology of the corroded Al 1070 alloy immersed in 1.0M HCl for 4h at RT for (a) annealed alloy and (b) Four passes ECAP.

3.2.2. Influence of extrusion at different speeds on the corrosion performance of Al 1070 alloy

The impact of extrusion at various speeds on the corrosion behavior of Al 1070 alloy, commonly used in automotive conductors, was investigated. The CR values obtained through the WL method for Al 1070 alloy extruded at different speeds in 0.2M HCl and 1.0M HCl at RT are depicted in Fig. 6. After 1h immersion in 0.2M HCl, the CR values for extrusion speeds of 1, 5, 10, and 15 mm/min are 454.6, 496.0, 702.6, and 785.3 mm/y, respectively. Correspondingly, after 4h immersion in 0.2M HCl, the CR values for the same speeds are 227.3, 310.0, 330.6, and 620.0 mm/y. For 1.0M HCl, the CR values after 1h immersion at different speeds are 826.6, 1405.2, 1735.9, and 3843.7 mm/y, while after 4h immersion, the CR values are 444.3, 516.6, 547.6, and 4443.0 mm/y, respectively. The CR values show an increase in the solution's acidity, transitioning from 0.2M HCl to 1.0M HCl. Moreover, an increase in immersion times results in decreased CR values, indicating the formation of a protective layer on the Al 1070 alloy. Optimal conditions are observed when extruded at a speed of 1 mm/min for both HCl concentrations.

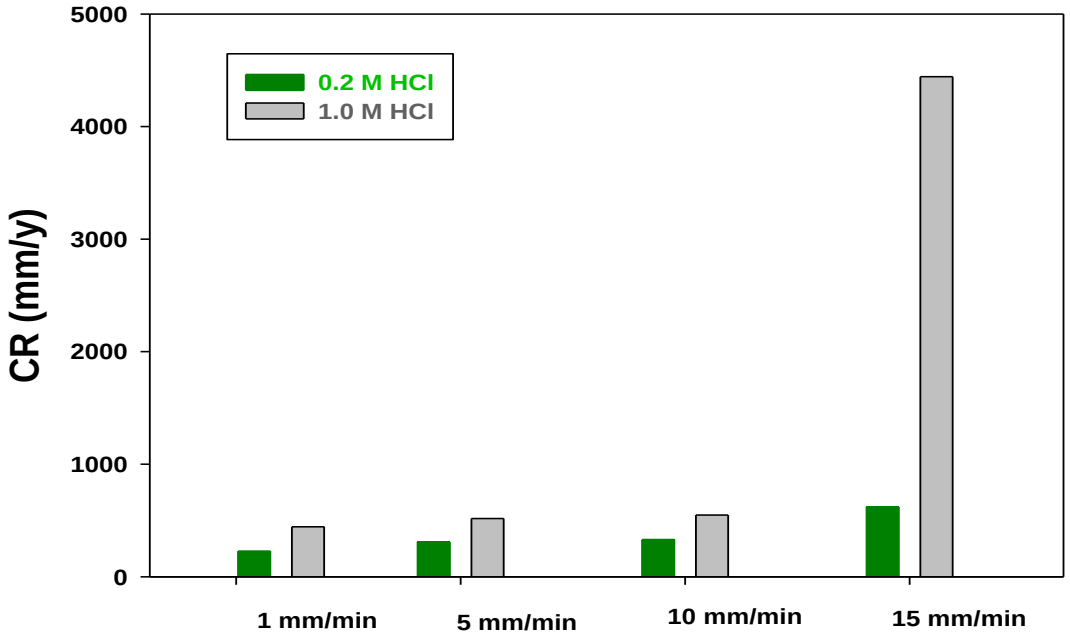

Fig. 6. The CR values of Al 1070 alloy at different speeds of extrusion immersed in 0.2M HCl and 1.0M HCl for 4h at RT.

The CR values obtained through the immersion of Al 1070 alloy, extruded at various speeds, in 3.5% NaCl for 1h and 4h at RT are illustrated in Fig. 7. After 1h immersion in 3.5% NaCl, the CR values for extrusion speeds of 1, 5, 10, and 15 mm/min are 372.0, 413.3, 620.0, and 702.6 mm/y, respectively. Correspondingly, after 4h immersion in 1.0M HCl, the CR values for the same speeds are 196.3, 217.0, 258.3, and 310.0 mm/y. The prolongation of immersion times results in an escalation of CR values, indicating the absence of a protective Al_2O_3 layer. The optimum corrosion resistance for both immersion periods is observed at an extrusion speed of 1 mm/min. Although higher extrusion speeds enhance productivity, they adversely impact corrosion resistance [44]. It is noteworthy that the CR values in 3.5% NaCl are lower than those in 0.2M and 1.0M HCl, attributed to the higher pH of 3.5% NaCl.

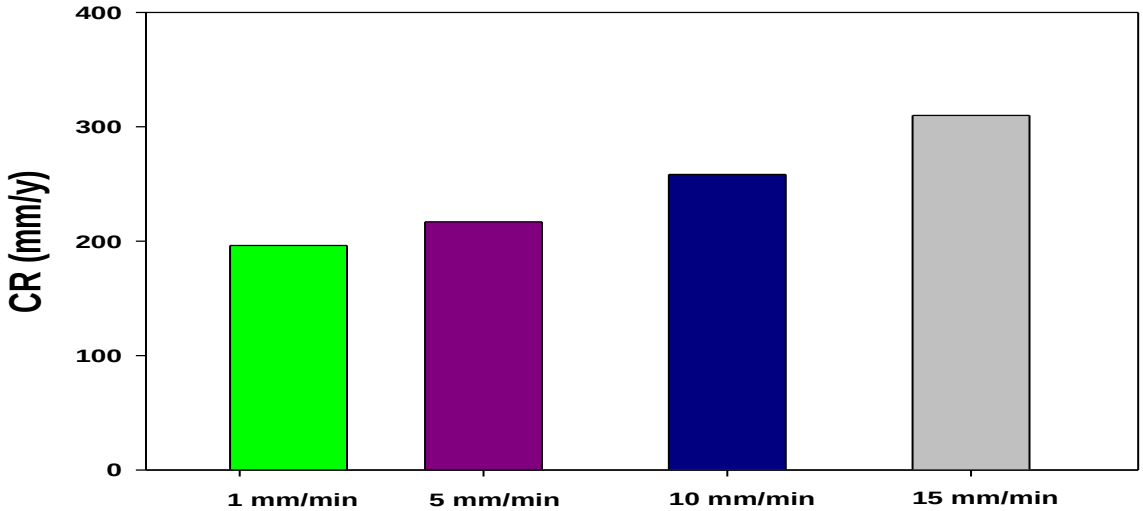

Fig. 7. The CR values of Al 1070 alloy at different speeds of extrusion immersed in 3.5% NaCl for 4h at RT.

The SEM morphologies of the corroded Al 1070 alloy in 1.0M HCl for 4 h at RT, specifically for extrusion speeds of 1 mm/min and 15 mm/min, are illustrated in Fig. 8. The corroded alloy extruded at a speed of 15 mm/min exhibits the most pronounced pitting corrosion. An observed trend is that as the extrusion speed increases from 1 to 15 mm/min, there is a corresponding increase in the WL to three times in 0.2M HCl and ten times in 1.0M HCl for a 4 h immersion time. This indicates that higher extrusion speeds are associated with more extensive pitting corrosion, particularly evident in the SEM images of the alloy extruded at 15 mm/min.

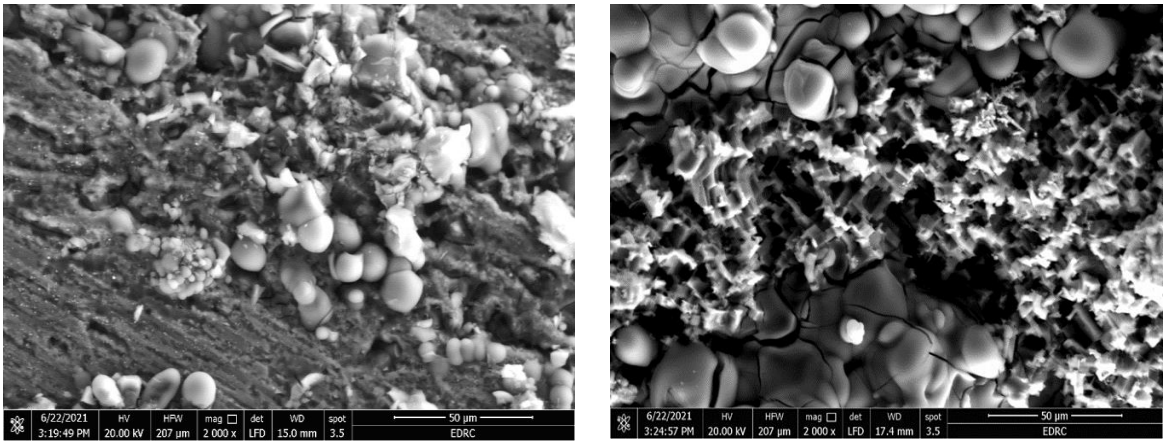

(a) (b)

Fig. 8 The surface morphologies of corroded Al 1070 alloy in 1.0M HCl for 4h at RT after extrusion with speed (a) 1 mm/min, and (b) 15 mm/min

3.2.3. Influence of extruded at different speeds on the corrosion characteristics of Al 1070 alloy of 4-pass ECAP samples.

The study investigated the impact of different extrusion speeds on the corrosion performance of Al 1070 alloy, specifically 4-pass ECAP samples intended for automotive conductors. The CR values, obtained through the WL method, for Al 1070 alloy extruded at various speeds are depicted in Fig. 9. For 4-pass ECAP samples after 1 h immersion in 0.2M HCl, the CR values at extrusion speeds of 1, 5, 10, and 15 mm/min are 805.94, 785.3, 454.6, and 826.6 mm/y, respectively. After 4 h of immersion in the same HCl concentration, the corresponding CR values are 444.30, 423.6, 310.0, and 475.3 mm/y. In 1.0M HCl, the CR values after 1 h immersion at the same

extrusion speeds are 1529.23, 1363.9, 1074.6, and 1322.6 mm/y, while after 4 h, they are 526.96, 495.7, 434.0, and 464.7 mm/y, respectively. The CR values exhibit a decreasing trend with increasing solution acidity from 0.2M HCl to 1.0M HCl. Moreover, extended immersion times contribute to reduced CR, indicative of the formation of a protective layer on the Al 1070 alloy. Intriguingly, at an extrusion speed of 10 mm/min, the 4-pass ECAP sample demonstrated the lowest CR in both HCl media. However, the CR values do not follow a clear trend with changes in extrusion speed for the 4-pass ECAP samples. This suggests that various factors, including internal stress from the 4-pass ECAP manufacturing process, grain refinement, and heightened mechanical properties (tensile strength and hardness), may contribute to the complex corrosion behavior observed [10-13].

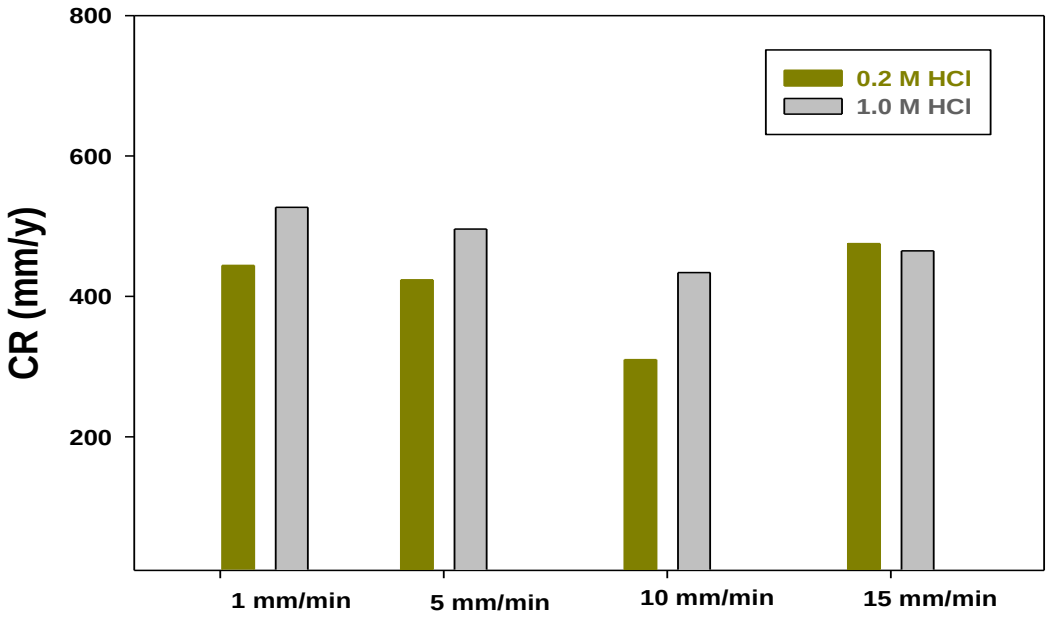

Fig. 9. The CR values of Al 1070 alloy at different speeds of extrusion immersed in 0.2M HCl and 1.0M HCl of 4-pass ECAP samples for 4h at RT.

The CR values, obtained through the WL method, for Al 1070 alloy extruded at different speeds and immersed in 3.5% NaCl for 1 h and 4 h at RT, are presented in Fig. 10. For 4-pass ECAP samples, the CR values after 1 h immersion in 3.5% NaCl at extrusion speeds of 1, 5, 10, and 15 mm/min are 1363.9, 826.6, 578.6, and 578.6 mm/y, respectively. After 4 h of immersion in 1.0M HCl, the corresponding CR values for the same extrusion speeds are 464.97, 413.3, 227.3, and 227.3 mm/y, respectively. The trend reveals that increasing immersion times results in higher CR values, indicating a lack of protective Al_2O_3 layer formation, as observed previously. The extrusion speed of 1 mm/min exhibits the lowest corrosion resistance among the various speeds for both immersion times in 4-pass ECAP samples. Extrusion speeds of 10 and 15 mm/min show identical CR values for the two immersion times. Additionally, the CR values in 3.5% NaCl are smaller than those in 0.2M and 1.0M HCl, attributed to the higher pH of 3.5% NaCl compared to the acidic HCl solutions.

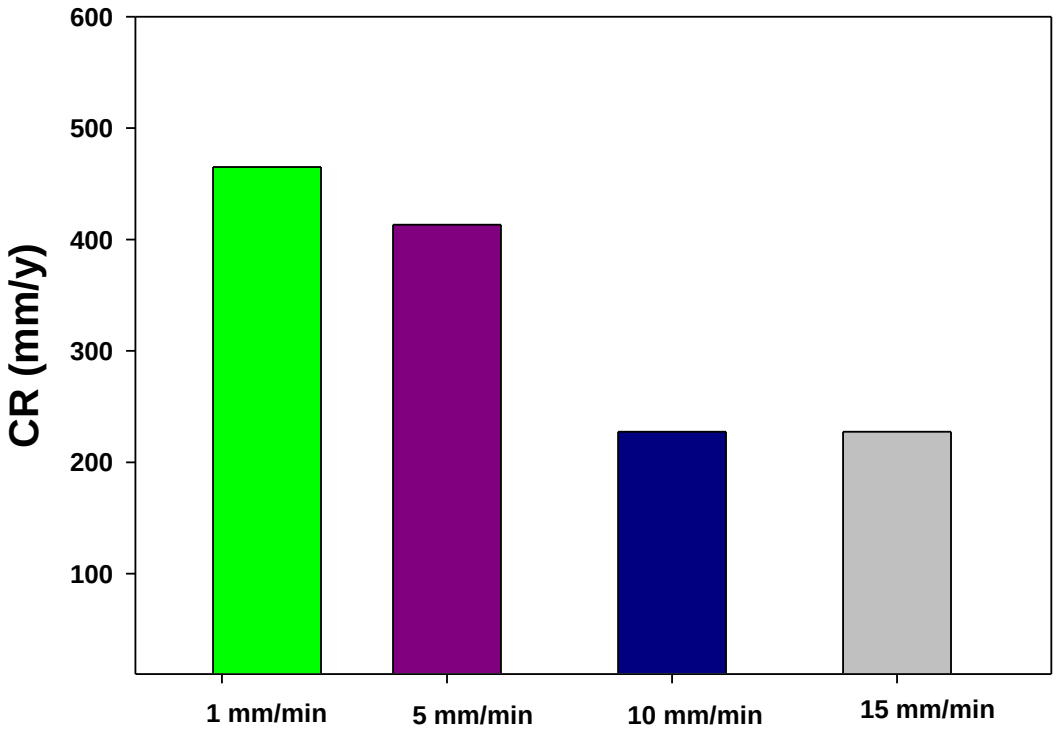

Fig. 10. The CR values of Al 1070 alloy at different speeds of extrusion immersed in 3.5% NaCl of 4-pass ECAP samples for 4h at RT.

4. Conclusions

The investigation delved into a comprehensive analysis of how various processes affect the corrosion characteristics of the Al 1070 alloy across different environments, namely 3.5% NaCl (pH=6.8), 0.2M HCl (pH=1.7), and 1.0M HCl (pH=0.8). In both 0.2M and 1.0M HCl solutions, the CR exhibited a remarkable tenfold decrease with just a single pass of ECAP in comparison to conventional annealing techniques. This phenomenon underscores the beneficial impact of the ECAP process, attributed to its role in facilitating the formation of a protective Al_2O_3 film, thereby bolstering the alloy's corrosion resistance. Interestingly, the lowest CR value was documented in the annealed alloy when exposed to 3.5% NaCl, suggesting nuanced variations in corrosion behavior across different environments. Moreover, as the number of ECAP passes increased from one to four, a substantial escalation in WL was noted, indicating a sixfold increase in 0.2M HCl and a sevenfold increase in 1.0M HCl during a 4 h immersion period. In 3.5% NaCl, this increase was comparatively modest at only 3.5 times. This disparity underscores the complex interplay between processing techniques and environmental factors in dictating corrosion behavior. Furthermore, elevating the extrusion speed from 1 mm/min to 15 mm/min resulted in a notable threefold increase in WL in 0.2M HCl and a remarkable tenfold increase in 1.0M HCl over a 4 h immersion period. The highest CR was recorded at 15 mm/min, contrasting with the lowest CR observed at 1 mm/min. Despite the enhanced productivity associated with higher extrusion speeds, this escalation led to a discernible decrease in corrosion resistance. Additionally, the morphological examination revealed the presence of pitting corrosion, with more pronounced manifestations observed in the annealed alloy compared to ECAP-treated specimens. At an extrusion speed of 15 mm/min, pitting corrosion exhibited a heightened severity compared to lower speeds, underscoring the nuanced influence of processing parameters on corrosion morphology. The corrosion behavior of specimens subjected to different extrusion speeds in the 4-pass ECAP samples exhibited no clear trend, owing to several factors such as internal stresses induced during manufacturing and grain refinement that influence corrosion resistance in different chloride media.

5. Conflict of interest

The authors declare that they have no conflicts of interest.

6. References

1. Z. Xu, L. Peng, P. Yi, X. Lai, An investigation on the formability of sheet metals in the micro/meso scale hydroforming process, Int. J. Mechan. Sci., 150 (2019) 265-276.
2. F. Vollertsen, H.S. Niehoff, Z. Hu, State of the art in micro forming, International Journal of Machine Tools and Manufacture, 46(11) (2006) 1172-1179.
3. U. Engel, R. Eckstein, Microforming—from basic research to its realization, J. Mater. Process. Technol, 125 (2002) 35-44.
4. K.M. Geiger M, Eckstein R, Tiesler N, Engel U, Microforming, CIRP annals, 50(2) (2001) 445-462.
5. F. Vollertsen, Z. Hu, H.S. Niehoff, C. Theiler, State of the art in micro forming and investigations into micro deep drawing, J. Mater. Process. Technol, 151(1) (2004) 70-79.
6. F. Vollertsen, Dirk Biermann, Hans Nørgaard Hansen, I. S. Jawahir, and Karl Kuzman, Size effects in manufacturing of metallic components, CIRP annals, 58(2) (2009) 566-587.
7. M. Yeh, H. Lin, H. Lin, C. Chang, Superplastic micro-forming with a fine grained Zn–22Al eutectoid alloy using hot embossing technology, J. Mater. Process. Technol, 180(1-3) (2006) 17-22.
8. W. Kim, Y. Sa, Micro-extrusion of ECAP processed magnesium alloy for production of high strength magnesium micro-gears, Scripta Materialia, 54(7) (2006) 1391-1395.
9. J. Xu, L. Shi, C. Wang, D. Shan, B. Guo, Micro hot embossing of micro-array channels in ultrafine-grained pure aluminum using a silicon die, J. Mater. Process. Technol., 225 (2015) 375-384.
10. W. Abdel-Aziem, A. Hamada, T. Makino, M.A. Hassan, Microstructure evolution of AA1070 aluminum alloy processed by micro/meso-scale equal channel angular pressing, Metal. Mater. Int., 27 (2021) 1756–1768.
11. W. Abdel-Aziem, A. Hamada, T. Makino, M.A. Hassan, Micro/Meso-Scale Equal Channel Angular Pressing of Al 10 70Alloy: Microstructure and Mechanical Properties, J. Mater. Eng. Perform., 29(9) (2020) 6201-6211.
12. W. Abd-Elaziem, M.A. Hassan, T. Makino, A. Hamada, Grain size affecting the deformation characteristics via micro-injection upsetting, Mater. Sci. Technol, (2021) 1-12.
13. W. Abdel-Aziem, A. Hamada, T. Makino, M. Hassan, Microstructural evolution during extrusion of equal channel angular-pressed AA1070 alloy in micro/mesoscale, Mater. Sci. Technol, (2020) 1169-1177.
14. S. Koch, H. Antrekowitsch, Aluminum Alloys for Wire Harnesses in Automotive Engineering, BHM Berg- Hüttenmänn. Monatshefte. 152 (2007) 62–67.
15. C.Rochet, M.Veron, E.F.Rauch, T.C.Lowe, B.Arfaei, A.Laurino, J.P.Harouard, C.Blanca, Influence of equal-channel angular pressing on the microstructure and corrosion behaviour of a 6xxx aluminium alloy for automotive conductors, Corros. Sci., 166, 15 2020, 108453
16. M. Murashkin, A. Medvedev, V. Kazykhanov, A. Krokhin, G. Raab, N. Enikeev, R.Z. Valiev, Enhanced Mechanical Properties and Electrical Conductivity in Ultrafine-Grained Al 6101 Alloy Processed via ECAP-Conform, Metals. 5 (2015) 2148–2164.
17. A. Awasthi, K.K. Saxena, R.K. Dwivedi, D. Buddhi, K.A. Mohammed, Design and analysis of ECAP Processing for Al6061 Alloy: a microstructure and mechanical property study, Int. J. Interact. Des. Manuf., (2023) 17, 2309–2321
18. E.A. El-Danaf, Mechanical properties, microstructure and texture of single pass equal channel angular pressed 1050, 5083, 6082 and 7010 aluminum alloys with different dies, Mater. Des. 32 (2011) 3838–3853.
19. M.H. Goodarzy, H. Arabi, M.A. Boutorabi, S.H. Seyedein, S.H. Hasani Najafabadi, The effects of room temperature ECAP and subsequent aging on mechanical properties of 2024 Al alloy, J. Alloys Compd. 585 (2014) 753–759.
20. Y. Duan, L. Tang, G. Xu, Y. Deng, Z. Yin, Microstructure and mechanical properties of 7005 aluminum alloy processed by room temperature ECAP and subsequent annealing, J. Alloys Compd. 664 (2016) 518–529.
21. R.Z. Valiev, T.G. Langdon, Principles of equal-channel angular pressing as a processing tool for grain refinement, Prog. Mater. Sci. 51 (2006) 881–981.
22. T. Khelfa, M.A. Rekik, J.A. Muñoz-Bolaños, J.M. Cabrera-Marrero, M. Khitouni, Microstructure and strengthening mechanisms in an Al-Mg-Si alloy processed by equal channel angular pressing (ECAP), Int. J. Adv. Manuf. Technol. 95 (2018) 1165-1177.
23. O. Sitdikov, E. Avtokratova, T. Sakai, Microstructural and texture changes during equal channel angular pressing of an Al–Mg–Sc alloy, J. Alloys Compd. 648 (2015) 195–204.
24. B. Adamczyk-Cieslak, J. Mizera, K.J. Kurzydlowski, Microstructures in the 6060 aluminium alloy after various severe plastic

deformation treatments, Mater. Charact. 62 (2011) 327–332.
25. Y. Zheng, B. Luo, Z. Bai, J. Wang, Y. Yin, Study of the Precipitation Hardening Behaviour and Intergranular Corrosion of Al-Mg-Si Alloys with Differing Si Contents, 7 (2017) 387–399.
26. G. Svenningsen, M.H. Larsen, J.H. Nordlien, K. Nisancioglu, Effect of high temperature heat treatment on intergranular corrosion of AlMgSi(Cu) model alloy, Corros. Sci. 48 (2006) 258–272.
27. D. Zander, C. Schnatterer, C. Altenbach, V. Chaineux, Microstructural impact on intergranular corrosion and the mechanical properties of industrial drawn 6056 aluminum wires, Mater. Des. 83 (2015) 49–59.
28. G. Fadel, L.Z. Mohamed, G.A. Gaber, O.A. El kady, A. Elhabak, M. Adly, S.A. Abolkassem, Evaluation of corrosion and wear features of Al matrix reinforced with particles (SiC+Y2O3) coated with either nano-Ag/Ni or nano/Ag/Cu, Egypt. J. Chem., 67 (2024)
29. G.A. Gaber, A. Abdelfattah, L.Z. Mohamed, A comprehensive investigation of corrosion efficiency of Cu-10Ni alloy in hybrid Cr3+/ Ni2+ with tungstate in chloride media, Egypt. J. Chem., 67 (2024).
30. W. Abdel-Aziem, M.A. Hassan, T. Makino, A. Hamada, Microstructure, Mechanical Properties of Extruded Aluminum at Different Ram Speeds in Micro/Meso-Scale, Metallography, Microstructure, and Analysis 10(4) (2021) 402-409.
31. D. Song, A. Ma, J. Jiang, P. Lin, D. Yang, Corrosion behavior of ultra-fine grained industrial pure Al fabricated by ECAP, Trans. Nonferrous Met. Soc. China. 19 (2009) 1065–1070.
32. K.D. Ralston, N. Birbilis, C.H.J. Davies, Revealing the relationship between grain size and corrosion rate of metals, Scr. Mater. 63 (2010) 1201–1204.
33. M.I. Abd El Aal, M.M. Sadawy, Influence of ECAP as grain refinement technique on microstructure evolution, mechanical properties and corrosion behavior of pure aluminum, Trans. Nonferrous Met. Soc. China. 25 (2015) 3865–3876.
34. H. Miyamoto, Corrosion of Ultrafine Grained Materials by Severe Plastic Deformation, an Overview, Mater. Trans. 57 (2016) 559–572.
35. J.G. Brunner, N. Birbilis, K.D. Ralston, S. Virtanen, Impact of ultrafine-grained microstructure on the corrosion of aluminium alloy AA2024, Corros. Sci. 57 (2012) 209–214.
36. K.D. Ralston, D. Fabijanic, N. Birbilis, Effect of grain size on corrosion of high purity aluminium, Electrochimica Acta. 56 (2011) 1729–1736.
37. S.H. Kim, U. Erb, K.T. Aust, Grain boundary Character distribution and intergranular corrosion behavior in high purity aluminium, Scripta Mater. 44 (2001) 835–839.
38. B. Zaid, D. Saidi, A. Benzaid, S. Hadji, Effects of pH and chloride concentration on pitting corrosion of AA6061 aluminum alloy, Corros. Sci., 50(7) (2008) 1841–1847.
39. W.R. Osorio, L. C. Peixoto, P. R. Goulart, A. Garcia, Electrochemical corrosion parameters of as-cast Al-Fe alloys in a NaCl solution, Corros. Sci., 52(9) (2010) 2979–2993.
40. R. Ambat, A.J. Davenport, G.M. Scamans, A. Afseth, Effect of iron-containing intermetallic particles on the corrosion behaviour of aluminium, Corros. Sci, 48(11) (2006) 3455–3471.
41. I. Son, H. Nakano, S. Oue, S. Kobayashi, H. Fukushima, Z. Horita, Effect of Equal-Channel Angular Pressing on Pitting Corrosion of Pure Aluminum, Int. J. Corros., (2012) 450854.
42. G.A. Gaber, W.A. Hussein, W.A. Ghanem, Nanoparticles deposition effects on 1050A aluminum alloy anodic layers, Mater. Res. Express, 7 (2020) 016567
43. L. Romero-Resendiz, J.M. Cabrera, S. Elizalde, V. Amigo-Borras, I.A. Figueroa, G. Gonzalez, Mechanical, stress corrosion cracking and crystallographic study on flat components processed by two combined severe plastic deformation techniques, J. Mater. Res. Technol., 18 (2022) 1281-1294.
44. A. Aytac, B. Dascilar, M. Usta, The effect of extrusion speed on the structure and corrosion properties of aged and non-aged 6063 aluminum alloy, Mater. Chem. Physics 130 (2011) 1357–1360.